Geophysical pre-investigation for a Stockholm tunnel project

Joint inversion and interpretation of geoelectric and seismic refraction data in an urban environment

Ronczka, Mathias; Wisén, Roger; Dahlin, Torleif

Published in:
Near Surface Geophysics

DOI:
10.3997/1873-0604.2018009

2018

Document Version:
Publisher's PDF, also known as Version of record

Near Surface Geophysics, 2018, **16**, 258-268 doi:10.3997/1873-0604.2018009

Geophysical pre-investigation for a Stockholm tunnel project: joint inversion and interpretation of geoelectric and seismic refraction data in an urban environment

Mathias Ronczka[1*], Roger Wisén[2] and Torleif Dahlin[1]

[1] *Lunds Universitet - Engineering Geology, Box 118 Lund 221 00, Sweden*
[2] *Ramboll Group A/S Ringgold standard institution, Kobenhavn, Hovedstaden, Denmark*

ABSTRACT

Underground constructions for public traffic purposes are becoming increasingly important for urban areas in order to use the limited space more efficiently. Several electric resistivity tomography and seismic refraction tomography measurements were performed crossing a water passage near Stockholm during the pre-investigation phase of a tunnel building project. The objective was to determine the bedrock interface and qualitatively assess the rock quality. The scope of this study is to present a field case in an urban environment and show improvements of geophysical results due to additional model constraints by a joint inversion. Results of individual inversions show a large transition zone below the seabed from electric resistivity tomography. Some parts of the seismic refraction tomography have a low model resolution, due to gas-bearing sediments with a low velocity together with a high noise level, which leads to insufficient investigation depth that makes it difficult to determine the bedrock interface. However, the bedrock interface could be reconstructed in the resistivity model by performing a joint inversion, using the seismic velocity model to constrain the electric resistivity tomography model and vice versa. Adjacent geotechnical soundings support the joint inversion results. A vertical low resistive zone could be identified as a dominant fracture zone in the southern part of the investigated area. In general, the joint inversion approach significantly improved the electric resistivity tomography results and provided a more reliable bedrock estimation.

Key words: ERT, SRT, Seismic refraction, Joint inversion, Urban geophysics.

INTRODUCTION

Due to limited space and environmental considerations, more infrastructures are nowadays being placed underground. This has resulted in an increasing demand for the urban underground infrastructure projects. Several tunnels crossing water passages are planned to be constructed in Stockholm, Sweden, in the near future, including motorway tunnel systems, underground metro line, a sewage tunnel and a high-voltage power supply tunnel (Wichmann 2018). Good knowledge about the underground properties is essential to avoid delays and unforeseen costs in underground infrastructure construction projects. One of the most important aspects in the planning and pre-investigation phase to reduce risk is to locate the bedrock surface and the zones of weak and water-bearing rocks. Areas of interest are underwater passages, since these are generally located over major weakness zones. The bedrock depth is usually estimated by geotechnical drillings, which provide detailed but only point information. Furthermore, drilling on water requires extensive logistics and is expensive, which risks limiting the amount of drilling. According to the National Research Council (1996), the standard methods for fracture detection range from geological explorations at the surface to seismic and electromagnetic soundings. They state that geophysical methods cover three different scales: (i) large scale, (ii) intermediate scale, and (iii) small scale, which include surface-to-borehole and borehole-to-borehole soundings and measurements directly adjacent to a borehole or tunnel. Geophysical investigations can also be used to provide continuous models of the subsurface and provide the base for integrating information from geotechnical point investigations. If geophysics is used in an early stage, the results can be used for planning the drilling programme and to ensure that zones of high risk are properly investigated. The geotechnical drilling information is also used as validation of the geophysical results. The combination of drilling information with geophysical measurements can, in turn, be used to refine the interpretation and to integrate point information into 2D or even 3D.

An example of a successful weakness zone detection using electric resistivity tomography (ERT) is the Hallandsås tunnel (Dahlin, Bjelm and Svensson 1999), which was constructed in the late 1990s during a railway tunnel project. Nevertheless, geophysical measurements in an urban environment are more difficult and

* mathias.ronczka@tg.lth.se

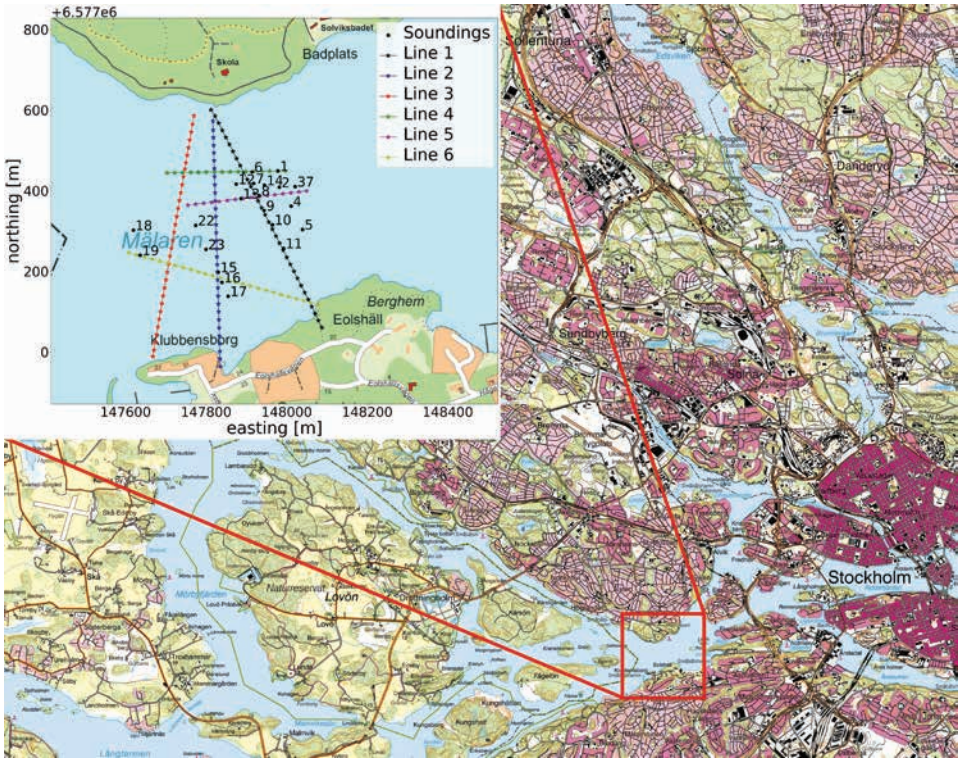

Figure 1 Map of Stockholm showing the area of investigation (red rectangle). The inlet shows the positions of the profile lines, together with geotechnical soundings marked with white circles. ERT and SRT lines are shown for each profile (© Lantmäteriet, data base: GSD-terrain map, scale: 1:50000).

should be treated carefully. Urban environments usually exhibit a high noise level, especially when it comes to seismic measurements. To counter the poor signal-to-noise ratio, Malehmir *et al.* (2015) suggests to perform measurements during periods of reduced noise, like weekends or night-time. However, getting permissions for blasting during the night can be difficult. It can be necessary to conduct ERT measurements during night-time if, for example, railways (public transport) are present. However, often, a higher noise level can be countered by adapting the measurement protocol and/or data processing. Recent progress in processing ERT full-waveform data by Olsson *et al.* (2016) increased the reliability and quality of estimated data. They use harmonic de-noising together with a series of filters to extract direct current (DC) and induced polarisation (IP) signals even for low signal-to-noise conditions. Additionally, dipole combinations with a low measurement voltage can be avoided/removed at further data processing steps.

Several investigations were conducted for transport administrations throughout Scandinavia (Dahlin *et al.* 1999; Lindstrøm and Kveen 2004; Ha, Kim and Park 2010; Karlsrud, Erikstad and Snilsberg 2003; Rønning *et al.* 2013), which integrated point information along the investigated lines. Although they provide less resolved information in depth, they give an overview of the investigated site and can predict possible parameter changes due to the presence of weakness zones, changed geology or weathering.

Lately, the use of joint inversion approaches are increasingly being used (e.g., Gallardo and Meju 2004; Linde *et al.* 2006; Doetsch, Linde and Binley 2010; Juhojuntii and Kamm 2015; Moorkamp *et al.* 2016). Common to all algorithms is the main assumption of a correlation of different geophysical parameter for different geological features. The joint inversion algorithm that is used in this study is based on a robust modelling method and was first mentioned by Günther and Rücker (2006), combining ERT and seismic refraction tomography (SRT) data. Generally, the algorithm allows exchanging structural model information and, thus, follows a structural scheme. Later, Günther *et al.* (2010) showed that the same algorithm can also be applied to other geophysical methods like DC/IP and magnetic resonance sounding. A more detailed description of the algorithm and extensive tests on synthetic cases were finally given by Hellman *et al.* (2017). They also investigated the influence of the different parameters in the coupling equation, which is used for calculating the elements of the weighting matrix.

A successful application of this approach for an underwater survey was presented by Ronczka *et al.* (2017). They show that a combination of geophysical methods increases the reliability and reduces the ambiguity of the results and, thus, eases the geological interpretation. A major advantage is the increased imaging properties by exchanging structural information between the used models that lead to a better imaging of sharp boundaries by ERT. Another successful investigation combining ERT and SRT measurements via joint inversion in an urban area is presented by Cardarelli *et al.* (2009). Their objective was to locate buried cavities in the city of Rome.

The geophysical survey presented here was originally conducted by Rambøll Denmark A/S on behalf of Stockholm Water in the urban area of Stockholm. The main objective was to investigate the

subsurface for weakness zones due to fracturing, weathering, or dykes to support a structural geologic interpretation and to map the bedrock surface. Individual and joint inversions were performed and compared to point out improvement due to a structural coupling during inversion. Geotechnical soundings that provided the bedrock depth were used for validation and, subsequently, for an integrated 2D model of the bedrock surface. This paper presents an example of better imaging of the sharp boundary towards the bedrock using structurally coupled joint inversion of SRT and ERT data.

TEST SITE

SRT and ERT measurements were conducted in the southern part of Stockholm across the water passage between Hägersten and Ålsten (see Figure 1). As part of the site investigation for a sewage tunnel, the main objective was to investigate the subsurface with focus on the bedrock depth and possible weakness zones in order to decide where to place the tunnel. Together with ERT and SRT measured on six lines, geotechnical soundings were available that gave information on the bedrock depth at several points within the investigated area. A bathymetry model was used to determine heights of sensor positions at the seabed. The seabed topography in most of the area has been surveyed in accordance with the highest International Hydrographic Organization standards (International Hydrographic Organization 2008) using a multi-beam echo sounder and is assumed to be accurate with a height error of a few centimetres. However, a part of the area was surveyed with single beam measurements that were verified and calibrated using the results from the multi-beam survey. A maximum water depth of 35 m was measured in the investigated area, whereas the average is 33.5 m along the profiles.

General geologic conditions show a complex pattern of fault zones in the Stockholm area. Past geological periods led to tectonic movements of the bedrock, leading to fractures and crushed zones (Morfeldt 1993). Fault zones reach an extent of several hundred kilometres. During the ice ages in the Quaternary age, an ice shield up to 3000 m thick covered the bedrock (Morfeldt 1993). As the last ice retreated slowly, in the years 20000–10000 BC, the bedrock began to rise, which is known as the isostatic land uplift. The upward movement declines form the northern towards the southern part of Sweden, until it is actually sinking. However, the Stockholm area still has a land uplift of about 50 cm per century. According to Morfeldt (1993), large boulders and rocks transported in the bottom of the ice scratched and sculptured the rock during the glacial period. Thus, the topography may show U-shaped valleys and trough-shaped depressions along fault zones. Quaternary deposits consisting of eroded splintered and weathered rock fragments were primarily deposited in topographical low levels during deglaciation, where the till is lying closest to the rock (Morfeldt 1993). That is why the topography consists of small hummocks, which are separated by sedimentary filled valleys. The overview of the general geologic conditions in Figure 2 shows a rather complicated pattern at the test site. Four major crushed or fracture zones cross each other at the centre of the investigated area. Three of them strike SW–NE, whereas one strikes NW–SE. In addition, several minor fracture zones appear throughout the southern area.

Stockholm is situated at Lake Mälaren. From a topographical point of view, Stockholm lies at the eastern end of a trough, which influenced the infrastructure significantly. The bedrock is of pre-Cambrian age and consists of metamorphosed rock like gneisses and migmatites and plutonic rocks ranging from gabbro to granite (Persson 1998). The granite of the Stockholm type is massive and fine to medium grained. Generally, the bedrock is hard and impervious; the groundwater usually flows through fissures, fractures, and crushed zones. The bedrock is intersected by dolerite dykes with a WNW to NW trend. Morfeldt (1993) describes that, under Swedish climate conditions, the bedrock type consisting of gneisses and granites is highly resistant to weathering. The fact that outcrops still show scratches by the retreated ice from the last glacial period supports this.

From an engineering point of view, the exact location of possible water-bearing fracture zones and continuous information about the bedrock depth is most important. However, the geologi-

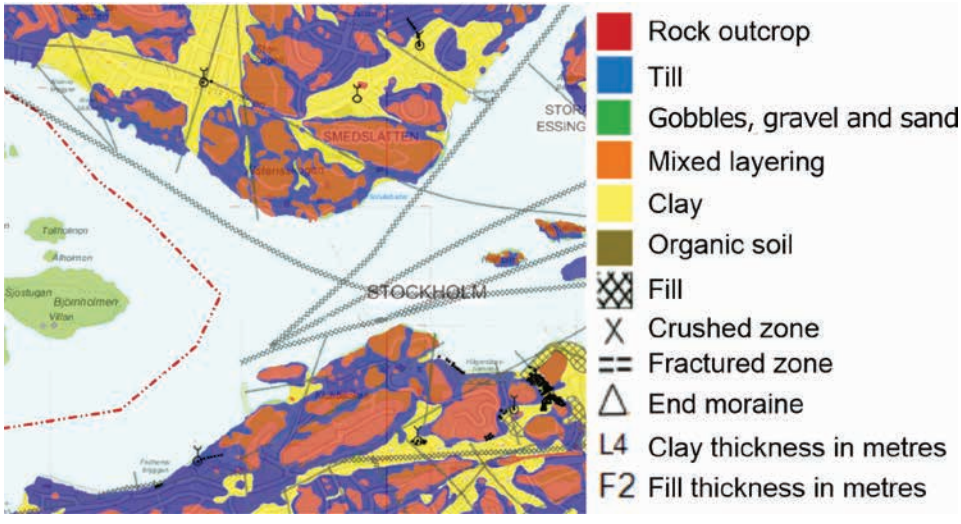

Figure 2 General geological overview about the test site showing the rock outcrops, till and clay layers, and crushed/fracture zones (https://iservice.stockholm.se/open/GeoArchive/Pages/Search.aspx , last access: 08.09.2017).

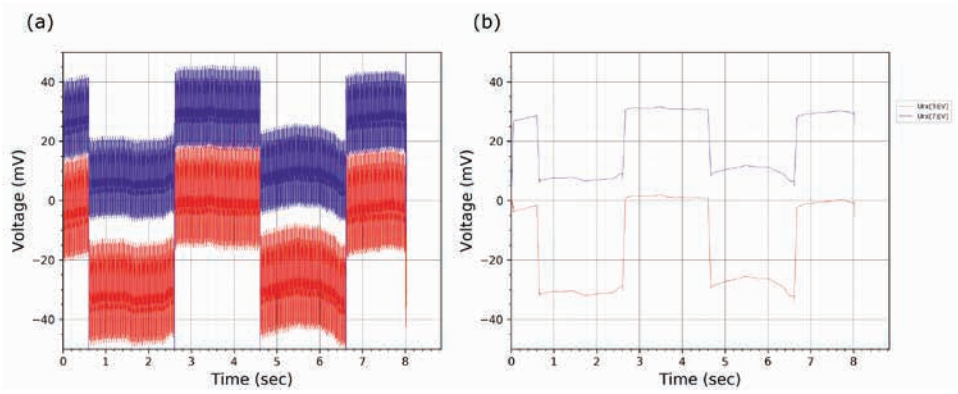

Figure 3 Example of a full-waveform data recording for profile 1, showing (a) raw data and (b) an average over 60 ms (16.7 Hz).

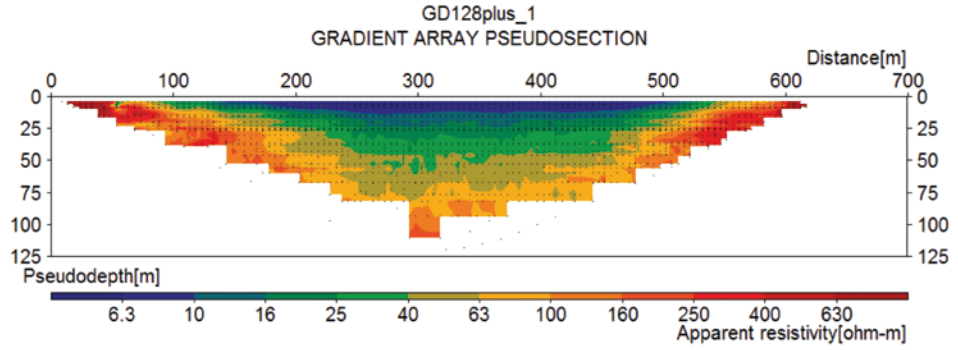

Figure 4 Pseudo-section of apparent resistivities for profile 1.

cal conditions in this area lead to the assumption that high resistivity contrasts can occur between quaternary deposits and unfractured bedrock. ERT mostly images sharp boundaries insufficiently due to the smoothness constrained inversion, which is usually performed. Therefore, additional constraints are needed. Seismic surveys on different scales are often used for detecting fracture zones (National Research Council 1996). As the resolution depends on the wavelength or frequency content of the seismic signal, it is possible that narrow fracture zones cannot be imaged with a seismic survey covering one scale. Thus, it can be problematic to image fracture zones just with the two mentioned methods alone. A combination, where the structural information of SRT confines the ERT inversion, can lead to better results.

METHODOLOGY

Coinciding ERT and SRT measurements along six profiles were performed covering a water passage. Individual inversion were done on all six and joint inversions on three of the profiles. The results of the different inversion approaches were compared with each other and with geotechnical soundings to show the benefit of the structural-based joint inversion.

Electric resistivity tomography

Two underwater electrode cables with 64 open take-outs each with an electrode spacing of 5 m were used. The cables had been placed on the sea bottom. The outtakes were connected to plate electrodes or stainless steel rods on the onshore part. The inset of Figure 1 shows that profiles 1 to 3 are approximately in N–S direction with a length of about 615 m and, three, in E–W direction. Geoelectric data were recorded using the ABEM Terrameter LS with 12 measuring channels along with an ABEM Electrode Selector ES10-64C in order to handle up to 128 electrodes. To ensure an efficient measuring progress, a multiple-gradient array (Dahlin and Zhou 2006) was used with a tailored measurement protocol to obtain good depth penetration. The protocol used all odd a-spacing multiples with an s-factor of 7, which means that the current electrode separation was nine times the potential electrode spacing. In addition, a number of measurements with larger s-factors were included for the longest electrode separations. All data were recorded with two stacks in full-waveform mode from which DC data were extracted. The water resistivity was measured as function of depth from the seabed up to the water surface at several points along the profiles. For this, the Terrameter was connected to a borehole cable with 32 electrode take-outs with 1-m spacing. A Wenner array was used to perform the water resistivity measurements.

The original dataset was collected, processed, and reported to Stockholm Water by Rambøll Denmark A/S. This report presents a first overview over standard inversion results for all lines but is not available to the public. A more detailed analysis for line 6 is given by Lindvall and Larsson (2016), which is a master's thesis work evaluating the combined use of ERT and SRT in infrastructure projects. For the work presented here, the pre-processed data from Rambøll has been made available. In general, the data are of good quality even though the ERT data were collected at daytime. Although significant noise is evident in the full waveform record-

ings, it was possible to extract useful DC data after processing the full-waveform data. The example in Figure 3 shows the 16.7-Hz noise that is removed by averaging. It also shows a low variation of the background level that remains. This is most likely caused by an external source, possibly the underground metro train system that runs on DC, since it is coherent in two measuring channels. The magnitude of the background trend varies for different data points.

Between 1400 and 3700 data points were recorded per profile, depending on the profile length. For each profile, between 0.1% and 20.7% of all data points were removed based on analysis of outliers and standard deviation. The amount of data points before and after the processing is given in Table 1 for each profile. The processed pseudo-section (profile 1) is shown in Figure 4.

GNSS positions of the electrodes were taken while the cable was laid out. The positioning error for the sensor positions at the lake floor is difficult to estimate. Due to low current of the water and careful cable handling during the profile preparation, the error is assumed to be approximately 1 m. That assumption is based on the GPS accuracy, the behaviour of the water current, and experiences from similar work. If available, the analysis of reciprocal measurements can provide a good error estimation (Udphuay *et al.* 2011), but since reciprocal data are more prone to noise for nested arrays, this might lead to an overestimation of errors. Furthermore, time constraints did not allow taking reciprocal measurements for this survey. Therefore, an error model consisting of a 4% relative error and 0.3-mV absolute error was used. The lake water resistivity was around 70 Ωm with little variation with depth, whereas the minimal apparent resistivity (ρ_a) measured at each profile ranges between 3 Ωm and 10 Ωm. Hence, it is evident that low resistive sediments below the lake bottom influence the measured ρ_a values strongly. In contrast, the maximal ρ_a ranges between 200 Ωm and 70,000 Ωm, depending whether the profiles shown cover a land part and if there are rock outcrops or not.

Seismic refraction tomography

As for the resistivity data, all seismic data were collected, processed, and provided by Rambøll Denmark A/S. Seismic streamer cables with 48 hydrophones and 5-m spacing were placed on the lake floor, resulting in a maximum offset of 235 m. Longer profiles were measured in a roll-along mode with one hydrophone overlap. Two 24-channel Geodes from Geometrics were used to record data.

Table 1 Amount of data points before and after the processing for each ERT profile.

Line	Full dataset	Edited dataset	Percent removed
1	3667	2907	20.7%
2	3711	3697	0.4%
3	3711	3265	12.0%
4	1376	1367	0.7%
5	1376	1374	0.1%
6	2752	2573	6.5%

Only P-wave signals were gathered with the used equipment. Thus, in the following discussions, the velocity refers only to the P-wave velocity. The signals were generated with 25- to 50-g Pentex explosives. Shotpoints were placed every 20 m along the profiles. The time window was set to 512 ms with a sample interval of 31.25 µs. On line 1, SRT measurements were performed during daytime. However, the data quality was not sufficient and it was decided to collect further data during night-time. The raw data example for profile 1 in Figure 5a shows poor signal-to-noise conditions that lead to higher uncertainties for estimating first arrivals, especially for traces 1040–1048. Figure 5b shows that conducting SRT measurements during the night at profile 2 lead to a significantly better data quality.

Data processing and extraction of first arrival times was done with Rayfract (vers. 3.33 Permanent Pro) from Intelligent Resources Inc. The SRT and ERT lines are not strictly coincident. They might have different start and end positions, and in case of profile 1 and 6 in Figure 1, SRT and ERT were measured in opposite directions. Therefore, mapping and shifting sensor positions were part of the data processing for the joint inversion because the sensors of both methods must be on the same line or coinciding in order to generate a common mesh. Picked first arrival times for profiles 1 (left) and 6 (right) are shown in Figure 6.

According to the first arrival times shown in Figure 6, no refracted wave appears for several shots, especially for the whole second half of profile 1 (for approximately x = 300–600 m). The same can be seen for several shots at profile 6 as well. Thus, a low investigation depth can be expected for those parts.

Joint inversion

This section describes briefly the joint inversion algorithm that was used in this study. The main assumption common to all joint inversion algorithms is a correlation between the used parameters, in this case, electrical resistivities and seismic velocities. That means, if one variable increases for a geological unit, the other one decreases (negative) or increases (positive). The input parameter for all conducted inversion (individual and joint) is slowness and logarithms of resistivities. The algorithm is based on reweighting the smoothness operator/derivative matrix **C**. The number of rows in **C** equals the number of boundaries and is given as follows:

$$\mathbf{C} = \mathrm{diag}(\mathbf{w})\mathbf{C}_0. \quad (1)$$

Here, the vector **w** holds weighting factors w_i, which are applied to the normal smoothness operator $\mathbf{C}_0$ (without weighting). This can be used to alter the model by controlling the contrast and its direction and include, for example, isotropy (Coscia *et al.* 2011). Günther, Bentley and Hirsch (2006) and Günther *et al.* (2010) applied this reweighting method for a joint inversion by introducing a function for calculating the entries of **w**. This method also works on irregular meshes. The element-wise calculation is given as follows:

$$W_i = \left(\frac{a}{|r_i|+a} + b\right)^c . \quad (2)$$

In general, the parameters a, b, and c control the coupling strength. The influence of the coupling parameters (a, b, and c) is shown in detail by Hellman *et al.* (2017). The roughness **r** with its entries r_i contains the structural information (gradients) of a model. The elements of **w** are spanned in a diagonal matrix in which small values correspond to sharp boundaries. In general, a structurally coupled joint inversion finds and allows the enhancement of common structures and reducing the smoothing effects (Gallardo and Meju 2004).

The flow-chart in Figure 7 shows a schematic sketch of the joint inversion. At first, a mesh is generated, which is used for both methods. Several individual iterations are performed before the joint inversion is initiated. The purpose is to ensure a certain degree of structural information and model similarities that can be exchanged by the joint inversion, which usually do not appear after the first iteration. The default value is 4 individual iterations. However, it is also possible to run the individual inversion until the data are fitted within their errors, before initializing the joint inversion. As the joint inversion starts, the model roughness of each method is used to calculate the elements of the weighting vector **w** (entries of main diagonal diag(**w**) in equation (1)). Finally, the model roughness is updated with the weighting matrix and used for the next iteration step. This is going to be repeated until both datasets are fitted within their error. The ERT inversion is a standard smoothness constraint inversion described briefly by Hellman *et al.* (2017). The SRT inversion is a travel time estimation after Moser (1991), was used, known as the path method.

The TetGen (Si 2015) mesh generator was used to create finite-element (FE) meshes for inversion and forward modelling. All profiles are partly or entirely underwater. The water layer was assumed to be known during the inversion with a resistivity of 69 Ωm and a velocity of 1500 m/s. However, the water layer was decoupled from the model region. Note that in the following, all results are shown without the water layer. In order to obtain comparable results, joint and individual inversions were performed on the same mesh. Choosing the right mesh quality and refinement is important. The standard approach for ERT is to put one to two nodes equidistantly between adjacent electrodes, which leads to a sufficiently fine mesh at the surface. The mesh quality factor controls how fast the cells are growing with increasing depth by adding new points to the mesh. Additional quality constraints within TetGen control the angle ratio within a cell to avoid badly shaped (long and thin) cells. For SRT, we assumed a frequency content lower than 100 Hz when using explosives as a source. That leads to wavelengths of 10–60 m for velocities between

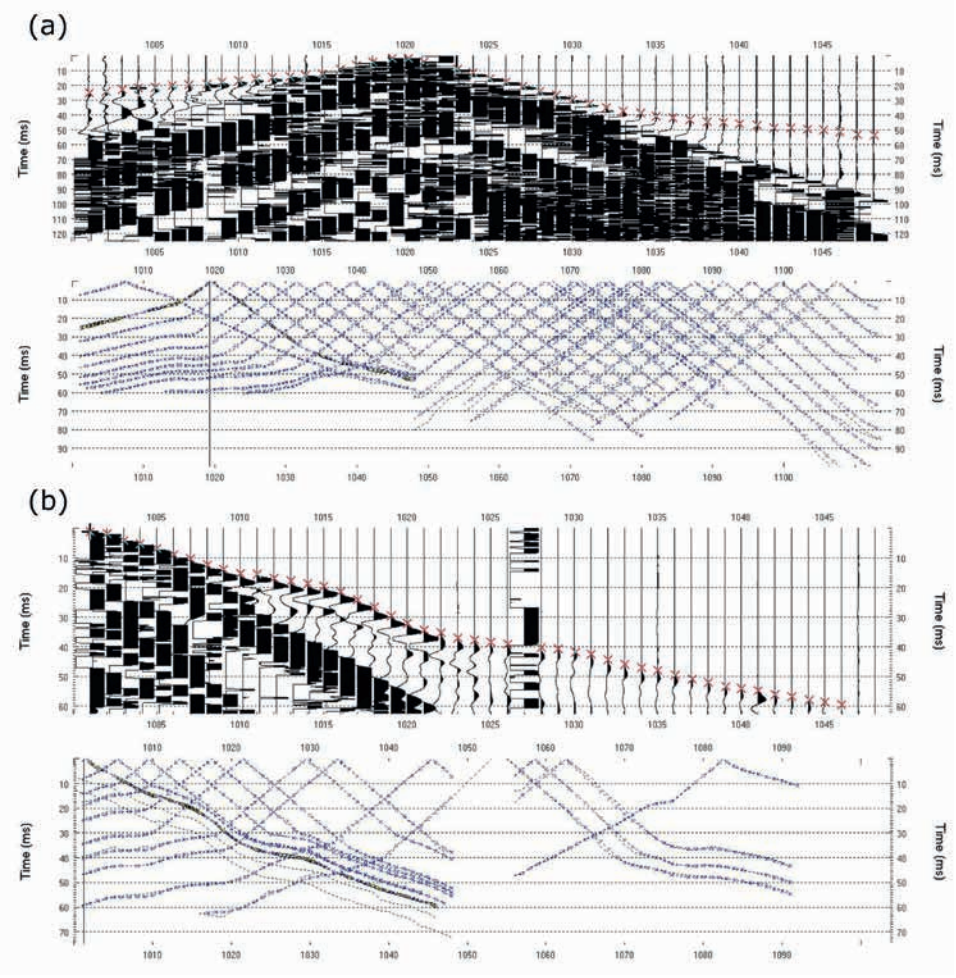

Figure 5 Seismograms (top) and picked first arrivals (bottom) for a part of (a) profile 1 measured during the day and (b) profile 2 measured at night.

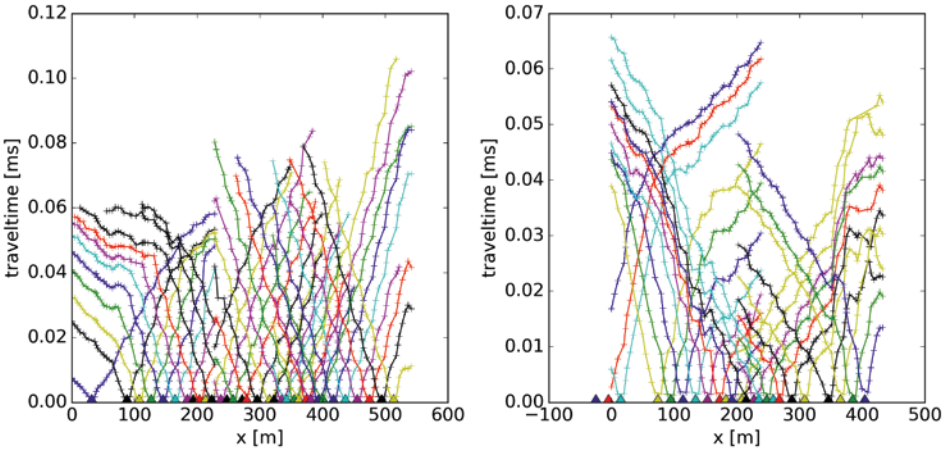

Figure 6 Picked first arrival times for profile 1 (left) and 6 (right). The shotpoints are marked with triangles.

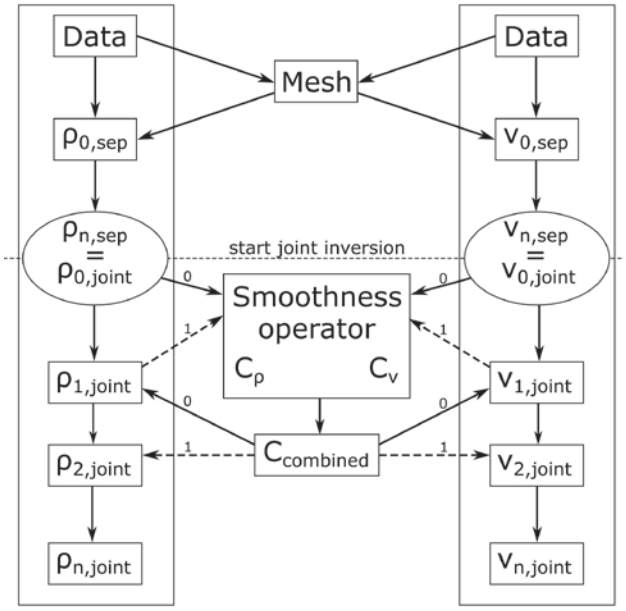

Figure 7 Flow-chart of the joint inversion (after Hellman et al. 2017) with the starting models of the individual inversions $\rho_{0,sep}$ and $v_{0,sep}$, their models after n iterations $\rho_{n,sep}$ and $v_{n,sep}$, the starting model of the joint inversion $\rho_{0,joint}$ and $v_{0,joint}$, and the final models $\rho_{n,joint}$ and $v_{n,joint}$. Hereby, ρ denotes the resistivity distribution and, v, the velocity distribution. The numbers 0 and 1 represent the zero and first iteration.

1000 m/s and 6000 m/s. With a minimal wavelength of 10 m, the best resolution is approximately 2.5 m, which is half the sensor (electrode, hydrophone) spacing. Conversely, that means the ERT mesh is fine enough for SRT. It was decided to use the electrode positions for the common mesh. Thus, the hydrophone positions had to be mapped to the electrode positions if necessary. That can lead to little variations of the direct wave but not the refracted. The used mesh for profile 1 is shown in Figure 8. It consists of three regions presenting the water (red), the parameter domain (yellow) on which the inversion is carried out, and the background (blue) which is needed to model electric fields accurately.

The coverage is calculated as the summation of all sensitivity values assigned to a model cell and is closely connected to the model resolution, which is also based on the sensitivity distribution as shown by Ronczka *et al.* (2017). For ERT, coverage-based thresholds are defined to separate regions of high, medium, and low reliability, which are not, partially or completely faded out when presenting inversion results. SRT uses a standardised coverage, which takes only the two values 0 and 1, depending if a ray travels through the cell or not. A smoothness-constrained inversion was performed until the data were fitted within their errors, that is $c^2 = F_d/N$. Standard initial models were used for the inversion, which is a homogeneous half-space with 1 Ωm for ERT and a layered subsurface with increasing P-wave velocity with depth.

RESULTS

The software package pyBERT/pyGIMLi (Rücker, Günther and Wagner 2017) was used for forward modelling and data inversion. ERT inversion results of all six profiles are shown in Figure 9. All profiles are individually and independently inverted. Note that the water level was set to z = 0 m and that the water layer is not shown in any result. It can also be noted that the relatively high resistivity of the lake water (70 Ωm) limits the influence of conductance in the water body, which makes the surveying conditions more favourable than in saline or brackish water. The resistivity distribution shows comparatively low resistivities for the bedrock. Only profile parts along the shore show resistivities above approximately 3000 Ωm. Although the resistivity distribution at intersecting points of most profiles matches quite well, it can be clearly seen that the intersections of profile 6 with the profiles 1 and 3 do not. A large transition zone appears for the underwater part, which makes it difficult to determine the bedrock depth. However, higher resistivities appear towards the shore at the northern and southern ends of the profiles, which is expected to be the bedrock. This could be visually validated at least at the onshore parts. The results also show a low resistive structure in the southern part of the test site. It strikes in EW direction and appears first at shallow depth at the beginning of profile 3 (southern part). It becomes more dominant in profile 2 at y < 100 m with an approximately vertical inclination and con-

tinues in profile 6 at x > 400 m. Note that the low resistive structure does not appear at profile 1.

Figure 10 shows the SRT results for all six profiles. Note that the SRT profiles are shorter compared with the resistivity measurements. As expected, the bedrock appears in all profiles as a high velocity zone with velocity > 4000 m/s (red parts). However, the velocity distribution within the bedrock is not homogeneous, which indicates possible variations in compactness, i.e., variation in bedrock quality or weathering degree. The interface towards the top low-velocity layer is mostly continuous. A thin zone of intermediate velocities between 3000 m/s and 4000 m/s appears on top of the bedrock. This is interpreted as weathered or crushed top bedrock. Several valley-shaped structures appear in profile 6, which are filled with sediments leading to low velocities below 3000 m/s (blue-coloured model part). Unreasonable velocities below 1500 m/s (assumed velocity of the water body) appear just in a small part of the model. As profile 4 is very short, the interface towards the bedrock does not almost appear because of the short shot-receiver offset. Profile 1 shows almost no model resolution in the southern part. The first arrivals shown in Figure 6 (left) indicate that no refracted wave appears for that part. For plotting purpose the profile had to be flipped because it was measured in the opposite direction. So the part with no refraction is between y = 150 m and 350 m in Figure 10, which is same in location with the part between x = 300 m and 600 m in Figure 6 left. It is assumed that gas-bearing sediments lead to a high seismic attenuation for this part. Additionally, a low seismic (refraction) signal quality made it difficult to pick first arrival times as this profile part was measured during daytime.

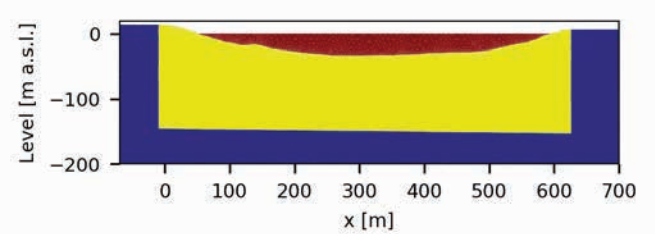

Figure 8 FE mesh used for data inversion of profile 1. The mesh is divided in three regions that mark the water (red), the background (blue), and the parameter domain (yellow).

A joint inversion was performed on profiles 1, 2, and 6, as their intersection covers the most critical part in the investigated area due to the crossing of several crushed or fracture zones. For comparison purposes, the individual inversions for those profiles were repeated using the same mesh as the joint inversion. The results for profile 1 are shown in Figure 11, with resistivity distributions for individual and joint inversion in (a) and (c) and velocity distributions in (b) (individual) and (d) (joint inversion). Geotechnical soundings, which mark the bedrock depth, are added as black circles. A comparison between Figure 11a and Figure 11c shows that the ERT inversion alone cannot image the bedrock interface, whereas the joint inversion result clearly shows the expected jump to high resistivities for the bedrock interface. The fact that the bedrock interface estimated by geotechnical soundings (−48.6 m to −56.5 m a.s.l.) is in the same depth range supports the joint inversion result. However, the interface in the joint-SRT result does not match well with the soundings below x < 300 m, which is probably caused by a low model resolution resulting from a low data coverage.

Figure 12 shows inversion results for profile 2. The bedrock depth estimation in the ERT result from the individual inversion in Figure 12a agrees with the geotechnical sounding as well as the joint inversion result in Figure 12c. In comparison to the ERT

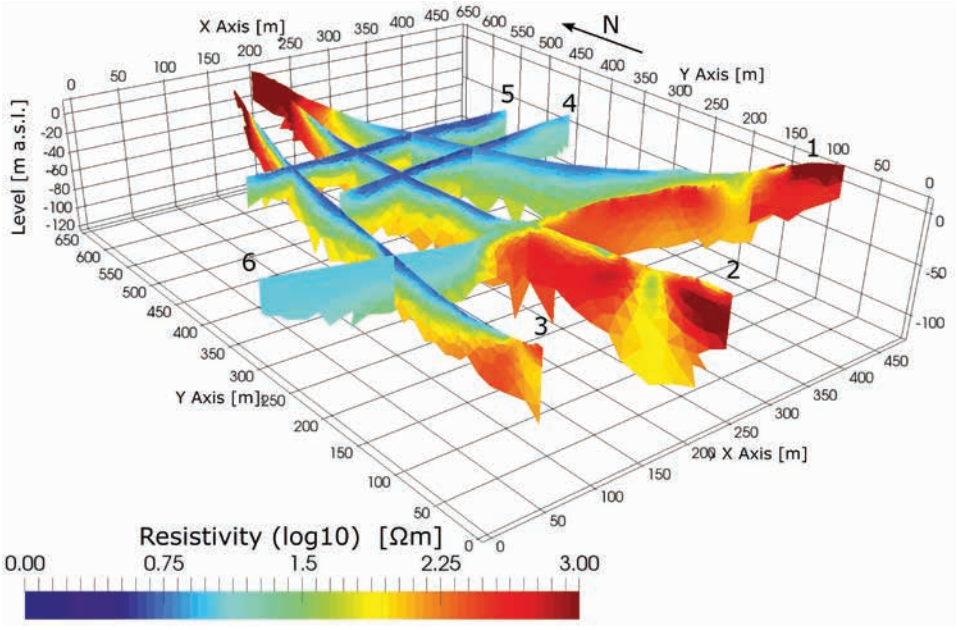

Figure 9 Inversion results for all six ERT profiles. The *y*-axis points in the north direction.

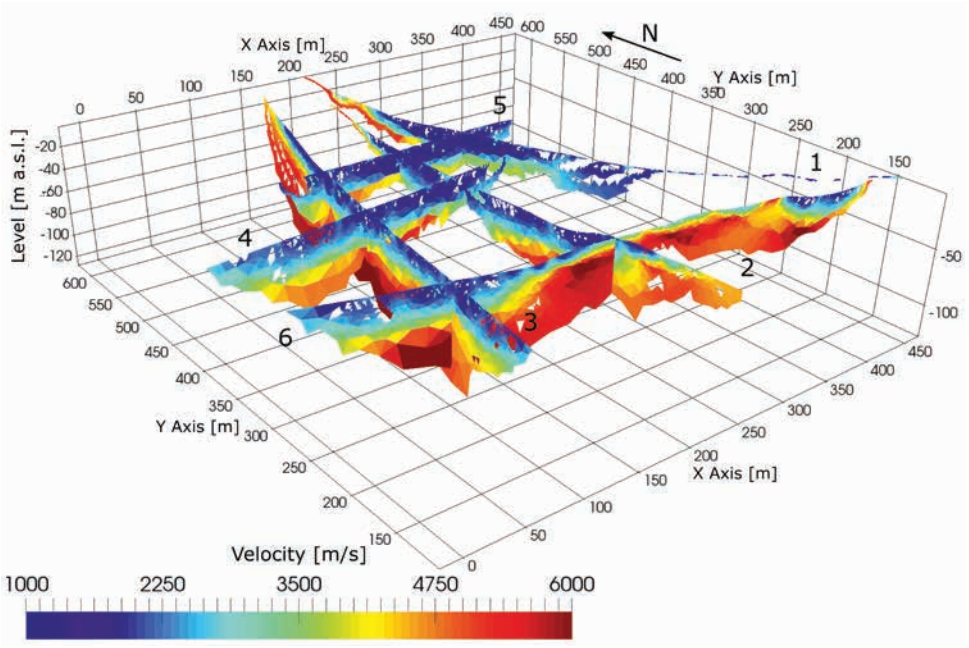

Figure 10 Result of the SRT data inversion for all six profiles.

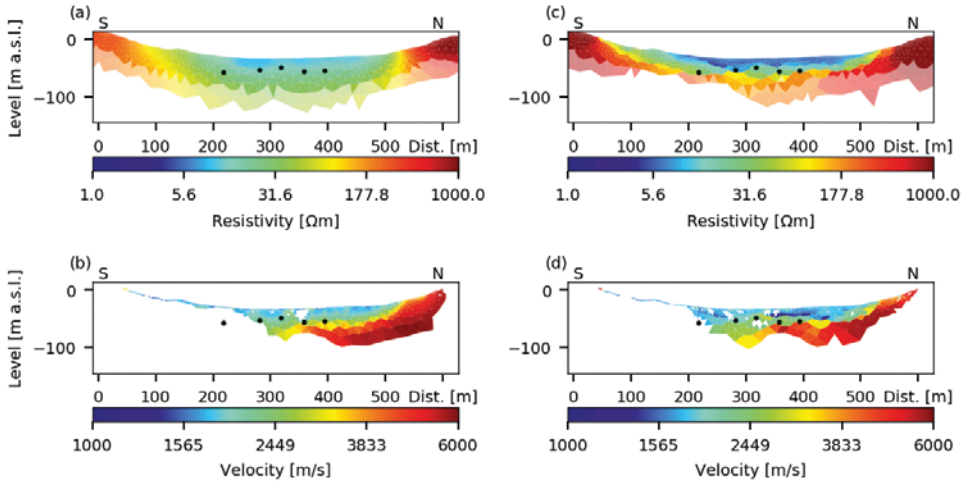

Figure 11 Inversion results of profile 1. Individual results are shown in (a) for ERT and (b) for SRT. The resistivity distribution of the joint inversion is shown in (c) and, the velocity distribution, in (d). Geotechnical soundings providing the bedrock depth are added as black dots.

results, the bedrock interface of the velocity distribution in Figure 12b is shifted to a larger depth. The interface towards the bedrock (velocities > 5000 m/s) between 400-m and 500-m distance is shifted from approximately −80 m up to −60 m by the joint inversion in Figure 12d. However, the interface still does not match with the ground truth given by the geotechnical sounding between 200-m and 300-m distance. The low velocity/resistivity zone between 100-m and 500-m distance and a depth above −50 m a.s.l., which is interpreted as sediments, show slight velocity variations. These are assumed to be inversion artefacts and not interpreted any further. The vertical low resistive zone in the southern part of the profile, at approximately 80-m distance, is interpreted as a possible water-bearing fracture zone. This is in accordance with geological information. However, SRT measurement on this profile does not cover the low resistive zone and, thus, gives no additional information.

The results for profile 6 for the individual inversions (a, b) and joint inversion (c, d) are shown in Figure 13. A valley-shaped zone of low resistivities and velocities below x = 100 m for the shallow part of the model appears, which is interpreted as a sediment-filled structure. For the offshore part (towards east), the same pattern occurs as in the profiles 1 and 2, which is a low resistive zone on top of a high resistive zone, that is a sediment covered bedrock. Figure 13a shows that the bedrock interface can hardly be identified when covered by a low resistivity zone because of the smoothness constraints of the inversion. The interface can only be resolved by adding structural constraints by the joint inversion as shown in Figure 13c. However, the interface depth is not matching well with the geotechnical sounding. Only slight differences between the individual inversion in Figure 13b and the joint inversion in Figure 13d for the SRT, like a sharpening of the bedrock interface, occur.

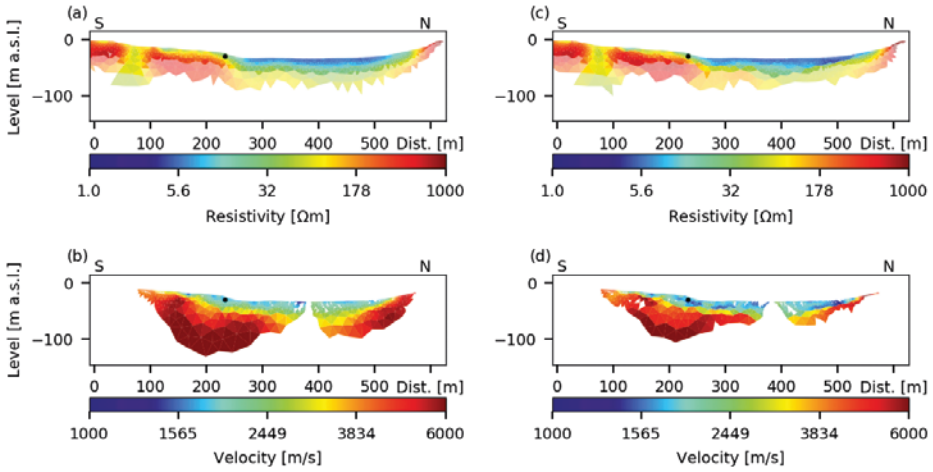

Figure 12 Results of profile 2 with the individual inversions showing (a) the resistivity and (b) the velocity distribution. The corresponding joint inversion results are given in (c) for ERT and, (d), for SRT. The black circle marks the bedrock depth from a geotechnical sounding.

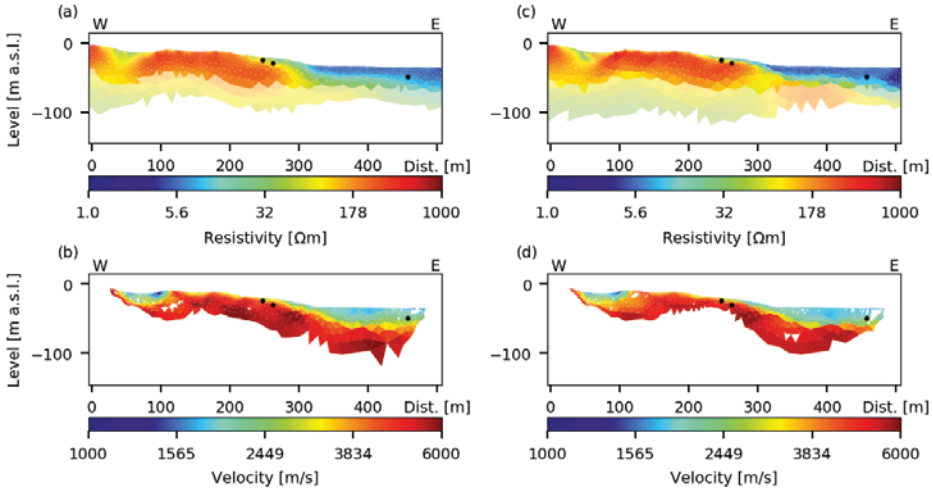

Figure 13 Inversion results of profile 6. Individual results are shown in (a) for ERT and (b) for SRT. The resistivity distribution of the joint inversion is shown in (c) and, the velocity distribution, in (d). Geotechnical soundings providing the bedrock depth are added as black dots.

CONCLUSIONS

Combined SRT and ERT measurements were made for a pre-investigation of a tunnel construction project authorised by Stockholm Water across a water passage. Measurements were performed along six profiles. The seismic data of the first profile revealed that measurements during daytime lead to data with a low signal-to-noise ratio, which makes it difficult to estimate first arrivals. Therefore, the rest of the survey was performed during the night, which is recommended for surveys in urban environments. A low resistive zone in the southern part of the investigated area could be identified as a possible fracture zone. The individual inversion results showed that the refraction seismic but not the ERT results could identify the bedrock depth. However, the quality of seismic signals was low for the first part of profile 1 and led to insufficient investigation depths due to a missing refraction. Thanks to exchanging structural information between the used methods by the joint inversion, the results could be significantly improved. The bedrock depth could be estimated by the ERT joint inversion result, also for parts that are poorly resolved by the seismic survey. The visual comparison with bedrock depths derived from geotechnical soundings (black circles in Figures 11, 12, and 13) shows a good agreement with two of the three performed joint inversions. In case of profile 2, the SRT part does not match the geotechnical sounding. However, all results show that the joint inversion finds equivalent models. It does not lead to drastically different models, which supports the stability of the algorithm. Thus, the reliability of the geophysical results could be improved, extrapolating the geotechnical point information into a continuous 2D image of the bedrock interface in this area. Although the interpreted southern fracture zone appeared thinner in the joint inversion result, it is still visible. It can be concluded that resulting subsurface models do not drastically change if a joint inversion is performed, but they are significantly enhanced. Particularly, ERT benefits from the additional structural information, which reduces the ambiguity of the results and leads, in this case, to higher resistivity contrasts for the bedrock interface. That proves the stability of the used approach and shows that structures can be imaged in more detail. Thus, for the pre-investigation of areas with a comparable geologic setting, it is recommended to consider ERT and SRT measurements and combine them in a joint inversion and interpretation together with soundings as a ground truth validation.

ACKNOWLEDGEMENT

The authors wish to thank Stockholm Water for making data from the field survey available and for giving permission to present the results. The authors thank Rambøll Denmark A/S and Ramböll Sweden AB for their support and for providing the authors with reference data. The authors also want to thank Elisabeth Lindvall and Erik Warberg for their excellent contributions, both during the field campaign in Lake Mälaren and through their thesis work. Funding, which made this work possible, was provided by BeFo, Swedish Rock Engineering Research Foundation (ref. 314 and 331, plus M.Sc. thesis support) and SBUF, The Development Fund of the Swedish Construction Industry (ref. 12718 and 12719). Formas, The Swedish Research Council for Environment, Agricultural Sciences and Spatial Planning, provided funding for this presentation of the results (ref. 2012-1931) as part of the Geoinfra-TRUST framework (http://www.trust-geoinfra.se/). Byggrådet provided additional funding that was essential for this study.

REFERENCES

Cardarelli, E., Gercato, M., Cerreto, A. and Di Filippo, G. 2009. Electrical resistivity and seismic refraction tomography to detect buried cavities. *Geophysical Prospecting* **58**, 685–695.

Dahlin, T., Bjelm, L. and Svensson, C. 1999. Use of electrical imaging in the site investigations for a railway tunnel through the Hallandsås Horst, Sweden. *Quarterly Journal of Engineering Geology* **32**, 163–173.

Dahlin, T. and Zhou, B. 2006. Multiple-gradient array measurements for multichannel 2D resistivity imaging. *Near Surface Geophysics* **4**, 113–123.

Doetsch, J., Linde, N. and Binley, A. 2010. Structural joint inversion of time-lapse crosshole ERT and GPR traveltime data. *Geophysical Research Letters* **37**, L24404.

Gallardo, L. A. and Meju, M. A. 2004. Joint two-dimensional DC resistivity and seismic travel time inversion with cross-gradients constraints. *Journal of Geophysical Research* **109**, B03311, *https://doi.org/10.1029/2003JB002716.*

Günther, T., Bentley, L. and Hirsch, M. 2006. A new joint inversion algorithm applied to the interpretation of DC resistivity and refraction data. *Proceedings of the 16th International Conference on Computational Methods in Water Resources*, Copenhagen, Denmark, June 19–22, 2006.

Günther, T., Dlugosch, R., Holland, R. and Yaramanci, U. 2010. Aquifer characterization using coupled inversion of DC/IP and MRS data on a hydrogeophysical test-site. 23rd EEGS Symposium on the Application of Geophysics to Engineering and Environmental Problems.

Günther, T. and Rücker, C. 2006. A new joint inversion approach applied to the combined tomography of dc resistivity and seismic refraction data. *19th EEGS annual meeting (SAGEEP)*, Seattle, WA.

Ha, H. S., Kim, D. S. and Park, I. J. 2010. Application of electrical resistivity techniques to detect weak and fracture zones during underground construction. *Environmental Earth Science* **60**, 723–731.

Hellman, K., Ronczka, M., Günther, T., Wennermark, M., Rücker, C., and Dahlin, T. 2017. Structurally coupled inversion of ERT and refraction seismic data combined with cluster-based model integration. *Journal of Applied Geophysics* **143**, 169–181.

International Hydrographic Organization 2008. *IHO Standards for Hydrographic Surveys*, 5th edn. Monaco: International Hydrographic Bureau, 28pp. (International Hydrographic Organization Special Publication, S-44).

Juhojuntii, N. and Kamm, J. 2015. Joint inversion of seismic refraction and resistivity data using layered models—Applications to groundwater investigation. *Geophysics* **80**, EN43–EN55.

Karlsrud, K., Erikstad, L. and Snilsbert, P. 2003. Tunnels for the citizens—Investigations of and restrictions on water leakage to maintain the environment. Tech. Rep. 103. Public Road Administration Oslo.

Linde, N., Binley, A., Tryggvason, A., Pedersen, L.B. and Revil, A. 2006. Improved hydrogeophysical characterization using joint inversion of cross-hole electrical resistance and ground penetrating radar traveltime data. *Water Resources Research* **42**, W12404.

Lindstrøm, M. and Kveen, A. 2004. Tunnels for the citizens——Final report. Tech. Rep. 105. Public Road Administration Oslo.

Lindvall, E. and Larsson, E. W. 2016. *Kombinerad förundersökning för tunnlar med resistivitet och refraktionsseismik i urban undervattensmiljö*. MSc thesis VTG820, Lund University, Dept. of Engineering Geology, ISRN LUTVDG/(TVTG-5145)/1–80/(2016), 80p.

Malehmir, A., Zhang, F., Dehghannejad, M., Lundberg, E., Döse, Ch., Friberg, O. *et al.* 2015. Planning of urban underground infrastructure using a broadband seismic landstreamer—Tomography results and uncertainty quantifications from a case study in southwestern Sweden. *Geophysics* **80**(6), B177–B192.

Moorkamp, M., Lelièvre, P.G., Linde, N. and Khan, M. 2016. Integrated imaging of the earth: theory and applications. *American Geophysical Union*.

Morfeldt, C.O. 1993. Underground construction on engineering geological terms: a fundamental necessity for the function of metropolitan environments and man's survival. *Engineering Geology* **35**, 149–165.

Moser, T.J. 1991. Shortest path calculation of seismic rays. *Geophysics* **56-1**, 59–67.

National Research Council 1996. *Rock Fractures and Fluid Flow: Contemporary Understanding and Applications*. *Chapter 4: Fracture Detection Methods*. Washington DC: The National Academies Press. *https://doi.org/10.17226/2309.*

Olsson, P.I., Fiandaca, G., Larsen, J.J., Dahlin, T. and Auken E. 2016. Doubling the spectrum of time-domain induced polarization by harmonic de-noising, drift correction, spike removal, tapered gating and data uncertainty estimation. *Geophysical Journal International* **207**, 774–784.

Persson, L. 1998. Engineering geology of Stockholm, Sweden. *Bulletin of Engineering Geology and the Environment* **57-1**, 79–90.

Ronczka, M., Hellman, K., Günther, T., Wisén, R. and Dahlin, T. 2017. Electric resistivity and seismic refraction tomography: a challenging joint underwater survey at Äspö Hard Rock Laboratory. *Solid Earth* **8**, 671–682.

Rønning, J. S., Ganerød, G., Dalsegg, E. and Reiser, F. 2013. Resistivity mapping as a tool for identification and characterisation of weakness zones in crystaline bedrock: definition and testing of an interpretational model. *Bulletin of Engineering Geology and Environment* **73**, 1225–1244.

Rücker, C., Günther, T. and Wagner, F.M. 2017. pyGIMLi: an open-source library for modelling and inversion in geophysics. *Computers & Geosciences* **109**, 106–123.

Si, H. 2015. TetGen, a Delaunay-based quality tetrahedral mesh generator. *ACM Transactions on Mathematical Software* **41**, 1–36.

Udphuay, S., Günther, T., Everett, M., Warden, R., and Briaud, J.-L. 2011. Three-dimensional resistivity tomography in extreme coastal terrain amidst dense cultural signals: application to cliff stability assessment at the historic D-Day site. *Geophysical Journal International* **185**, 201–220.

Wichmann, C. 2018. Att passera Saltsjö-Mälarsnittet med tunnel—En ny utmaning. *Proceedings of Grundläggningsdagen 2018*, Stockholm, Sweden, March 15, 2018, 8p.